Dilution of ^{10}Be in detrital quartz by earthquake-induced landslides: implications for determining denudation rates and potential to provide insights into landslide sediment dynamics

A. Joshua West[1]*, Ralf Hetzel[2], Gen Li[1], Zhangdong Jin[3], Fei Zhang[3], Robert G. Hilton[4], and Alexander L. Densmore[4,5]

[1] Department of Earth Sciences, University of Southern California, Los Angeles, CA 90089, United States

[2] Institut für Geologie, Westfälische Wilhelms-Universität, 48149 Münster, Germany

[3] State Key Laboratory of Loess and Quaternary Geology, Institute of Earth Environment, Chinese Academy of Sciences, Xi'an 710075, China

[4] Department of Geography, Durham University, Durham, DH1 3LE, United Kingdom

[5] Institute of Hazard, Risk and Resilience, Durham University, Durham, DH1 3LE, United Kingdom

*corresponding author: joshwest@usc.edu

Revised manuscript for consideration by *Earth and Planetary Science Letters*

Abstract

The concentration of ^{10}Be in detrital quartz ($^{10}Be_{qtz}$) from river sediments is now widely used to quantify catchment-wide denudation rates but may also be sensitive to inputs from bedrock landslides that deliver sediment with low $^{10}Be_{qtz}$. Major landslide-triggering events can provide large amounts of low-concentration material to rivers in mountain catchments, but changes in river sediment $^{10}Be_{qtz}$ due to such events have not yet been measured directly. Here we examine the impact of widespread landslides triggered by the 2008 Wenchuan earthquake on $^{10}Be_{qtz}$ in sediment samples from the Min Jiang river basin, in Sichuan, China. Landslide deposit material associated with the Wenchuan earthquake has $^{10}Be_{qtz}$ concentrations that are consistently lower than in river sediment prior to the earthquake. River sediment $^{10}Be_{qtz}$ concentrations decreased significantly following the earthquake downstream of areas of high coseismic landslide occurrence, because of input of the ^{10}Be-depleted landslide material, but showed no systematic changes where landslide occurrence was low. Changes in river sediment $^{10}Be_{qtz}$ concentration were largest in small first-order catchments but were still significant in large river basins with areas of 10^4-10^5 km^2. Spatial and temporal variability in river sediment $^{10}Be_{qtz}$ concentrations has important implications for inferring representative denudation rates in tectonically active, landslide-dominated environments, even in large basins. Although the dilution of $^{10}Be_{qtz}$ in river sediment by landslide inputs may complicate interpretation of denudation rates, it also may provide a possible opportunity to track the transport of landslide sediment. The associated uncertainties are large, but in the Wenchuan case, the ^{10}Be mixing suggests that river sediment fluxes in the 2-3 years following the earthquake increased by a similar order of magnitude in the 0.25-1 mm and the <0.25 mm size fractions, as determined from $^{10}Be_{qtz}$ mixing calculations and hydrological gauging, respectively. Such information could provide new insight into sediment transfer, with implications for secondary sediment-related hazards and for understanding the removal of mass from mountains.

Keywords: erosion; denudation; cosmogenic nuclides; landslides; Wenchuan earthquake; sediment

Highlights:

- ^{10}Be concentrations in quartz measured in the region of the 2008 Wenchuan earthquake, China
- river sediment ^{10}Be concentrations dropped due to input of landslide debris
- ^{10}Be-denudation rate estimates should consider high-magnitude, low-frequency events
- effect of landslides on ^{10}Be-denudation rates can be important even in large basins
- potential to infer sediment input from landslides and track its transport using ^{10}Be

1. Introduction

Accurately quantifying rates of erosion and sediment transport is vital to understanding mass redistribution processes at the Earth's surface, and how they relate to environmental and engineering hazards (e.g. Macklin and Lewin, 2003), regional to global-scale geodynamics and active tectonics (e.g. Willet, 1999; Attal and Lave, 2006; Parker et al. 2011), the biogeochemical systems that sustain life (e.g. Heimsath et al., 1997), and the function of the geological carbon cycle (e.g. West et al., 2005; Hilton et al., 2012). Over the past two decades, the use of cosmogenic radionuclides (CRNs) to determine denudation rates has provided a transformational new toolkit (Dunai, 2010), and the inventory of cosmogenic ^{10}Be produced *in-situ* in quartz grains ($^{10}Be_{qtz}$) collected from river sediment is now widely used to infer denudation rates averaged over the area of river catchments and over timescales of 10^2 to 10^4 years (Granger et al., 1996; von Blanckenburg, 2006; Portenga and Bierman, 2010).

In the $^{10}Be_{qtz}$ approach, the concentration of ^{10}Be in quartz grains is interpreted to reflect the integrated time that these grains have resided close to the Earth's surface. This is because ^{10}Be production is attenuated at depth in the Earth due to cosmic ray interaction with rock material, so that the ^{10}Be production rate is highest at the surface and decreases to negligible rates at a depth of several meters (e.g. Brown et al., 1995; Dunai, 2010). If the removal of material at the surface operates at a steady state, then determining the bulk $^{10}Be_{qtz}$ concentration in a sufficient number of detrital grains collected from river sediment can yield a representative catchment-averaged denudation rate (von Blanckenburg, 2006). Denudation rates determined in this manner are integrated over the time required for grains, on average, to move through the near-surface zone of ^{10}Be production.

81 The supply of sediment from bedrock landslides may generate an important non-steady state
82 perturbation to this averaging. This is because landslides can excavate material from both
83 within and below the near-surface zone of ^{10}Be production (Brown et al., 1995). By
84 delivering shielded, low-^{10}Be material to the river system, landslide sources are expected to
85 dilute $^{10}Be_{qtz}$ in river sediments (e.g. Niemi et al., 2005). These landslide inputs can
86 potentially complicate accurate determination of denudation rates in tectonically-active
87 settings, where information about erosion sheds valuable light on tectonic processes but
88 where landslide erosion is frequently the dominant hillslope denudation mechanism (e.g.
89 Hovius et al., 1997; Densmore et al., 1998). However, dilution of $^{10}Be_{qtz}$ by bedrock
90 landslide inputs may also present an opportunity to track the transport of landslide sediment
91 through mountain catchments – an important problem from engineering, hazard, and science
92 perspectives, but one that is non-trivial to tackle (e.g. Benda and Dunne, 1997; Cui et al.,
93 2003a, 2003b; Dadson et al., 2004).
94
95 The effects of stochastic and episodic landslide activity on river sediment $^{10}Be_{qtz}$ have been
96 considered theoretically (Niemi et al., 2005; Yanites et al., 2009; Ouimet, 2010), and some
97 recent empirical measurements have confirmed that river sediment $^{10}Be_{qtz}$ may be sensitive
98 to stochastic inputs, e.g. from debris flows (Vassallo et al., 2011; Kober et al., 2012).
99 However, there are little data to: (i) confirm in a systematic manner that landslide sources
100 actually contribute material with relatively low concentrations of ^{10}Be compared to
101 background (pre-landslide input) values in river sediment; and (ii) assess how and to what
102 extent the input of material as a result of a major landslide-triggering event may influence
103 the $^{10}Be_{qtz}$ signal in river sediments. In this study, we use the landslides triggered by the
104 2008 Wenchuan earthquake in Sichuan, China, to address this problem, by measuring ^{10}Be
105 concentrations both in landslide deposit material and in river sediment that has been
106 influenced by input from this high-magnitude, low-frequency event. We compare our post-

earthquake river sediment $^{10}Be_{qtz}$ data with results from samples collected at the same sites before the earthquake, and we explore the implications of the observed changes in $^{10}Be_{qtz}$ concentration for determining representative long-term denudation rates. We also consider the potential for the observed changes to contribute to understanding landslide sediment dynamics, although we acknowledge that the Wenchuan data leave large uncertainties in this application.

2. Setting: The 2008 Wenchuan Earthquake and Landslides

The M_w 7.9 Wenchuan (or Sichuan) earthquake (Hao et al., 2008) occurred on May 12th, 2008, along a series of dextral-thrust oblique-slip faults within the Longmen Shan, a mountain range that defines the eastern margin of the Tibetan Plateau and the northwestern edge of the Sichuan Basin. The earthquake triggered extensive coseismic landslides (e.g., Dai et al., 2010; Parker et al., 2011; Gorum et al., 2011; Xu et al., 2013; Ren et al., 2013; Li et al., 2014) and thus offers a valuable opportunity to explore the effect of widespread, impulsive delivery of landslide sediment to a fluvial network. Using remote sensing imagery collected over a time window of 1-6 months following the earthquake, we have recently produced a map of coseismic and immediately post-seismic landslides within the catchment area of the Min Jiang, which is the focus of this study (Fig. 1; Li et al., 2014). The Min Jiang is a principal tributary of the Yangtze River and one of the main rivers draining the Longmen Shan. It was the river with the largest drainage area to be acutely affected by Wenchuan earthquake-triggered landslides. The Min Jiang and its tributaries have incised deep valleys with high local relief (2-4 km) and steep slopes (angles often $>30^{o}$) across the dramatic topographic gradient of the Longmen Shan, which rises from the Sichuan Basin at ~500 m to peaks over 6000 m (Densmore et al., 2007; Ouimet et al., 2010; Zhang et al., 2011). The bedrock geology (Burchfiel et al. 1995; Robert et al., 2010; Burchfiel and Chen, 2012) is dominated by a Paleozoic passive margin sequence of

deformed metasediments intruded by granitic plutons, as well as Proterozoic granitoids and high-grade metamorphic rocks. The Heihe, Zagunao, and Yuzixi rivers, the major western tributaries of the Min Jiang, drain mainly granites and Songpan-Ganze flysch units, but show large contrasts in observed coseismic landslide areal density, defined here as area of landslide per unit catchment area (Fig. 1).

3. Methods

Following the Wenchuan earthquake, we collected samples from river sediments and landslide deposits for analysis of $^{10}Be_{qtz}$. For the landslide samples, we targeted a bedrock failure that is characteristic of the size of Wenchuan landslides and was accessible for sample collection from both the surface and interior of the deposit. In order to assess variability within landslide material, we collected two landslide sediment samples from different positions within the deposit (at the top of the surface and at the base of the deposit, exposed in cross section by road reconstruction) and one bedrock sample from the base of the exposed landslide scar. We targeted river sediment samples from sites where samples had been collected and analysed prior to the earthquake in 2004-2005 (Godard et al., 2010; Ouimet et al., 2009), with one additional sample from 2001 (Chappel et al., 2006). These sites included the Min Jiang River main stem, the Zagunao River, and the Yuzixi River, and 2 small first-order sub-catchments (Fig. 1; Table 1). Two of the sites were sampled twice as part of this study, in March 2009 and April 2010, and the others were sampled once in April 2010.

The stream and landslide sediment samples were washed, dried, and sieved into different grain-size fractions. To separate quartz for ^{10}Be analysis, we used the 0.25–1 mm size fraction from all river sediments, and the 0.25–2 mm fraction for the landslide sediment samples (JWS 09-2 and JWS 09-3). To evaluate grain-size effects, we also analysed the 1–4 mm fraction in three of the river sediment samples. The bedrock sample from the landslide

160 scar was crushed and sieved to 0.25-1 mm size. The respective size fractions of each sample
161 were split into magnetic and non-magnetic fractions with a hand magnet and a Frantz
162 magnetic separator. The non-magnetic fraction was etched once in 6 M HCl and three to
163 four times in diluted HF/HNO_3 in a heated ultrasonic bath to obtain clean quartz and
164 remove any meteoric ^{10}Be (Kohl and Nishiizumi, 1992). Final purification of the quartz was
165 achieved by two or three alternating etching steps in aqua regia and 8 M HF (Goethals et al.,
166 2009). After addition of ~0.3 mg Be-carrier, 40–50 g of quartz from each sample was
167 dissolved, and Be was separated on successive anion and cation exchange columns. The Be
168 was precipitated as $Be(OH)_2$ and transformed to BeO at 1000°C. Targets were prepared for
169 accelerator mass spectrometer (AMS) analysis at the AMS facility of ETH Zurich (Kubik
170 and Christl, 2010).
171
172 The areal density of landslides upstream of each river sediment sample was calculated from
173 the landslide inventory mapped by Li et al. (2014) based on remote sensing imagery. Total
174 landslide areas and areal densities were calculated as catchment-wide values, and as a
175 function of proximity to the river sampling site. For the latter calculation, the catchment
176 was divided into bands defined by 3 km increments along flow directions upstream from the
177 sampling sites; landslide area and areal density were both calculated within each band in
178 order to assess variability as a function of distance upstream from each sampling site.
179 Catchment boundaries and areas, and flow direction and accumulation maps, were
180 determined by flow routing using the hydrological algorithms in Grass GIS with SRTM
181 digital elevation data (Jarvis et al., 2008).
182
183 **4. Results**
184 ^{10}Be concentrations measured in quartz from the three samples from the landslide range
185 from 0.17 to 2.14 x 10^4 at/g (Table 1) and decrease from the bottom of the landslide

deposit up to the base of the exposed scar (Fig. 2). Concentrations range from 1.16 to 3.65 x 10^4 at/g in river sediment, with generally but not universally higher concentrations in samples from the small first-order catchments when compared to the larger river basins. Concentrations are systematically slightly lower (by 15-20%) in the coarser (1-4 mm) size fraction compared to the finer (0.5-1 mm) size fraction where both fractions were analyzed from river sediments.

Table 2 reports concentrations from samples collected after the Wenchuan earthquake (this study) and compares them to pre-earthquake data (Godard et al., 2010; Ouimet et al., 2009). The individual measurements for each sample time and site are shown graphically in Fig. 3. Only the data for the 0.25-1 mm size fraction are considered in this comparison, because complementary data on $^{10}Be_{qtz}$ in larger size fractions of river sediment from before the earthquake are not available. Large differences between pre- and post-earthquake sediment $^{10}Be_{qtz}$ (hereafter referred to as $\Delta^{10}Be_{qtz} = {}^{10}Be_{qtz,\ preEQ} - {}^{10}Be_{qtz,\ postEQ}$) are observed. Four of the six sites show a post-earthquake decrease in $^{10}Be_{qtz}$ that is greater than the reported analytical errors at the 2σ level (Table 2; Figs. 3, 4). The two sites that do not show statistically significant $\Delta^{10}Be_{qtz}$ (MJW and ZGN) at the 2σ level are those that have relatively little coseismic landslide activity upstream of the sampling site (Table 3; Figs. 3, 4). However, $\Delta^{10}Be_{qtz}$ is not a simple function of landslide areal density within the catchment area upstream of each sampling site (Fig. 4a). Variability in $\Delta^{10}Be_{qtz}$ is best explained if the location of landslides with respect to the basin outlet where sediments were collected is also considered (Table 3; Figs. 4b,c). For example, significant changes in $^{10}Be_{qtz}$ are observed for the main stem Min Jiang sampled near Yingxiu (site MJY), because of the very high landslide density immediately upstream of this sampling location (Fig. 4), even though the landslide density for the catchment as a whole is relatively low (Table 3).

Measured $^{10}Be_{qtz}$ in the landslide samples is lower than in pre-earthquake river sediment, as expected theoretically, but falls in a similar range to post-earthquake river sediment. The highest of measured landslide $^{10}Be_{qtz}$ is $2.14\pm0.21\times10^4$ at/g. Seven out of the eight pre-earthquake samples from the large rivers of the Min Jiang system (see Table 3, and additional data from Godard et al., 2010) are between 4.32 ± 1.26 and $7.55\pm1.19\times10^4$ at/g, and the small catchment data (Ouimet et al., 2009) are even higher. One river sediment sample reported by Godard et al. (2010), LM261, has a ^{10}Be concentration of $2.71\pm1.36\times10^4$ at/g. Although this value is still higher than our highest-concentration landslide sample, these two values cannot be distinguished statistically, given the uncertainties. However, the concentration reported for LM261 has an anomalously high uncertainty and is larger than the two other landslide samples we measured (at $0.95\pm0.12\times10^4$ at/g and $0.17\pm0.07\times10^4$ at/g).

5. Discussion

5.1. Empirical confirmation of low $^{10}Be_{qtz}$ in landslide material

The observed $^{10}Be_{qtz}$ in landslide material (Fig. 2) provide empirical data that confirm our expectations that Wenchuan landslides excavated shielded, low-$^{10}Be_{qtz}$ material via deep-seated failures. This is consistent with similar observations of low-$^{10}Be_{qtz}$ in landslides in Puerto Rico (Brown et al., 1995). Instantaneous excavation from depth yields relatively low ^{10}Be concentrations in the landslide sediment compared to pre-earthquake river sediment, because the latter (i) reflects material shed from hillslope surfaces that are ^{10}Be-rich because of less rapid hillslope erosion during interseismic periods (Parker et al., 2011) and (ii) may have accumulated additional ^{10}Be during fluvial transport to the sampling site (Anderson et al., 1996). The negligible ^{10}Be inventory at the base of the exposed scar (Fig. 2) indicates near-complete shielding prior to failure at the estimated pre-excavation depths of >5m where the scar was sampled. With only two data points, it is not clear whether the increase

238 from the top to the bottom of the deposit can provide any insight into failure dynamics (e.g.
239 with material that previously resided at the hillslope surface, carrying relatively higher ^{10}Be
240 concentrations, now at the bottom; see Fig. 2b). More systematic studies at higher
241 resolution and on a greater number of landslides would be needed to explore this question.
242
243 **5.2. Implications for determining denudation rates**
244 The input of previously-shielded landslide debris with comparatively low $^{10}Be_{qtz}$ is expected
245 to decrease the $^{10}Be_{qtz}$ in river sediment (Brown et al., 1995; Niemi et al., 2005; Yanites et
246 al., 2009; Ouimet, 2010; Kober et al., 2012). Our data provide direct empirical
247 demonstration of this effect associated with a single landslide-triggering event and suggest
248 that, to first order, higher total areas and areal densities of landslides leads to larger $\Delta^{10}Be_{qtz}$
249 (Figs. 3, 4). Total landslide area (km^2) and areal density (%) are not perfect metrics for
250 actual input of landslide material into the river network, partly because of the location of
251 landslides with respect to sampling sites (Fig. 4), and also because of variability in other
252 factors including deposit grain size, depth of failure, and connectivity to the river channel
253 network, which all may affect the extent to which a given landslide changes fluvial $^{10}Be_{qtz}$.
254 Nonetheless, it is clear from our data (Figs. 3, 4) that sampling sites with only very small
255 area of coseismic landslides in the upstream drainage do not show statistically significant
256 changes in $^{10}Be_{qtz}$, while those sites with substantial upstream landslide areas showed
257 significant decreases in in $^{10}Be_{qtz}$.
258
259 These observations have important consequences for determining representative long-term
260 erosion rates, because they mean that samples collected soon after a large event such as the
261 Wenchuan earthquake may overestimate the actual magnitude of denudation rates over the
262 timescales averaged by $^{10}Be_{qtz}$, while samples collected long after an event may
263 underestimate rates. For example, at the Yuzixi sampling site (YZX), the ^{10}Be

concentrations in river sediment quartz collected before the earthquake implied erosion rates of 0.64±0.19 and 0.59±0.17 mm/yr, for samples from 2004 and 2005, respectively (Godard et al., 2010); immediately after the earthquake, the implied long-term rates would have been 1.20±0.13 and 2.03±0.35 mm/yr (based on the $^{10}Be_{qtz}$ measured in samples JWS 09-04 and JWS 10-19, and an analogous production scheme and erosion rate calculation to that used by Godard et al., 2010). Similar differences (approximately threefold increases) are implied for the Min Jiang main stem at Yingxiu (MJY) and for one of the small catchments (SCLX), while smaller differences in denudation rate (roughly 1.5- to 2-fold increases) are implied for sites ZGN and SCMJ. The actual long-term averaged rate may lie somewhere in between the values that would be inferred from pre- and post-earthquake samples (as suggested by Ouimet, 2010). Note that the implicit averaging timescale of the estimated denudation rate also changes, in the case of the YZS site from ~800-1350 years based on samples from before the earthquake, to ~250-550 years based on the post-earthquake samples.

Models suggest that the input of landslide sediment may have a particularly significant effect on $^{10}Be_{qtz}$ in catchments with small areas (Niemi et al., 2005; Yanites et al., 2009). Indeed, the small first-order catchments in this study show some of the largest $\Delta^{10}Be_{qtz}$, consistent with the greatest sensitivity to the rates and volumes of stochastic landsliding. The models also show that such stochastic effects should average to yield a representative long-term denudation rate for a sufficiently large catchment area. It is tempting to view the mean area at which model basins tend to become well-averaged (~100 km^2; Niemi et al., 2005; Yanites et al., 2009) as a general threshold above which $^{10}Be_{qtz}$ is likely to yield a robust denudation rate, even in settings prone to mass wasting. However, the significant $\Delta^{10}Be_{qtz}$ seen in the large basins of the Min Jiang system, with catchment areas from 1000 to >10,000 km^2, indicates that cosmogenic nuclide samples from such large catchments may not necessarily always yield representative long-term denudation rates. This observation emphasizes that

290 there is a wide range around the mean value in the outputs of the stochastic models
291 simulating landslide effects on river sediment $^{10}Be_{qtz}$. Moreover, these models make
292 assumptions about landslides (e.g. magnitude-frequency relationships, area-volume scaling)
293 that may be generally representative in a globally-averaged sense but are not always
294 appropriate for all mountain belts. In particular, by averaging the effects of single high-
295 magnitude, low-frequency earthquakes or storms that trigger large landslide pulses, the mean
296 model outputs may underestimate the effect of events such as the Wenchuan earthquake.
297 Thus very significant changes in the ^{10}Be inventory may be expected in tectonically-active
298 settings even in large river systems, especially where the recurrence time of major
299 perturbations such as large earthquakes is long compared to the time it takes ^{10}Be
300 concentrations to return to pre-event levels. The importance of such changes for long-term
301 erosion rates will depend on return times of the high magnitude events.
302
303 In principle, river sediment $^{10}Be_{qtz}$ can also change over time when sediment source area
304 changes, if different source areas have different characteristic $^{10}Be_{qtz}$. In mountain
305 catchments, variability in source area $^{10}Be_{qtz}$ is expected because elevation differences
306 between tributaries lead to spatially variable ^{10}Be production rates. Year-to-year changes in
307 $^{10}Be_{qtz}$ from some rivers draining the south flank of the Nepalese Himalaya have been
308 attributed to the location of rainfall events, which may selectively sample headwater
309 sediment with variable $^{10}Be_{qtz}$ (Lupker et al., 2012). These effects were not observed in the
310 Min Jiang system prior to the Wenchuan earthquake, which instead showed constant $^{10}Be_{qtz}$
311 within uncertainty across multiple years (Godard et al., 2010). Moreover, sourcing effects are
312 not likely to explain the observed post-earthquake changes in the Min Jiang, because these
313 are observed across a range of scales (from small, first-order catchments to very large river
314 basins) and are temporally and spatially associated with landslide occurrence.
315

316 The Wenchuan data also highlight the important role for the location of landslides relative
317 to sampling sites in determining $\Delta^{10}Be_{qtz}$ associated with an earthquake. Where landslide
318 areal density is highest close the sampling site, $\Delta^{10}Be_{qtz}$ is generally larger (Table 2, Figs. 3,
319 4). Thus, in addition to potentially biasing the inferred magnitude of long-term denudation
320 rates, landslide activity may introduce significant spatial heterogeneity that may or may not
321 reflect actual spatial differences in denudation. Inferences about spatial variations in
322 denudation rates, increasingly used to address fundamental questions about tectonic systems
323 (e.g., Wobus et al., 2005; Densmore et al., 2009; Godard et al., 2012; Scherler et al., 2013;
324 Godard et al., 2014), may in some cases be convoluted if spatial variability reflects the
325 duration since the last major landslide-triggering event rather than more tectonically
326 meaningful long-term denudation rates. The importance of such event-driven spatial
327 variability is likely to depend on the return time and spatial distribution of landslide-
328 triggering events, and on the recovery time of the erosional system. However, spatial
329 variability in landslide occurrence may help to explain discrepancies in inferred erosion rates
330 at different spatial scales in some regions. For example, in the case of the Longmen Shan,
331 erosion rates inferred from cosmogenic nuclide measurements prior to the earthquake were
332 significantly lower in small first-order catchments than in the Min Jiang main stem and its
333 principle tributaries (Godard et al., 2010; Ouimet, 2010). The $\Delta^{10}Be_{qtz}$ observed in this study
334 as a result of the earthquake was larger for the small first-order catchments, bringing the
335 $^{10}Be_{qtz}$ values for these small basins closer to the large river values, and suggesting that the
336 pre-earthquake scale-discrepancy may have been at least in part related to the time since the
337 last large event (as hypothesized by Godard et al., 2010 and Ouimet, 2010).
338

339 **5.3. $^{10}Be_{qtz}$ as a tracer of landslide-derived sediment**

340 Quantifying the post-earthquake transport of landslide-derived sediment has presented a
341 major challenge in its own right. The magnitude, pattern and longevity of the sediment wave

342 from coseismic landslides have important implications for secondary hazards, because
343 sediment chokes river channels, causes flooding and infrastructure damage, and clogs
344 reservoirs (e.g., Huang and Fan, 2013). The transport of landslide sediment also influences
345 large-scale orogenic processes, because removal of landslide debris is an important mass flux
346 out of mountains (Hovius et al., 2011; Parker et al., 2011; Li et al., 2014). Most previous
347 work on transport of landslide sediment has relied on measurements of suspended sediment
348 fluxes collected at river gauging stations (e.g., in Taiwan: Dadson et al., 2004; Hovius et al.,
349 2011; Yanites et al., 2010, 2011; in Sichuan: Wang et al., *in review*). This approach is
350 limited by the available river gauging datasets and usually captures a selective grain size
351 range. The dilution of $^{10}Be_{qtz}$ by landslide material may provide an additional,
352 complementary opportunity to trace the transport of landslide-derived sediment, but has not
353 been previously explored.
354
355 One possible approach for quantifying Wenchuan landslide inputs to the fluvial system is
356 illustrated in Fig. 5. The mass of sediment being transported in the river following the
357 earthquake (M_{post}) can be calculated as a ratio to the pre-landslide sediment volume (M_{pre})
358 based on end-member mixing:
359
360 $$M_{post}/M_{pre} = (^{10}Be_{qtz,pre} - {}^{10}Be_{qtz,landslide})/(^{10}Be_{qtz,post} - {}^{10}Be_{qtz,landslide}) \quad (1)$$
361
362 where $^{10}Be_{qtz,pre}$ is the river sediment $^{10}Be_{qtz}$ concentration before the earthquake (known for
363 each site), $^{10}Be_{qtz,post}$ is the river sediment $^{10}Be_{qtz}$ concentration after the earthquake (also
364 known for each site), and $^{10}Be_{qtz,landslide}$ is the $^{10}Be_{qtz}$ concentration of the landslide material.
365 $^{10}Be_{qtz,landslide}$ is not precisely known because of variability in landslide material, both within
366 and between landslides (cf. Fig. 2). Fig. 5 shows estimated M_{post}/M_{pre} as a function of the
367 value of $^{10}Be_{qtz,landslide}$, for each of the sites in this study with significant $\Delta^{10}Be_{qtz}$. The

368 propagated analytical uncertainties lead to large possible ranges in M_{post}/M_{pre} but still clearly
369 show that M_{post}/M_{pre} is much higher in some catchments (e.g. MJY, YZX) compared to
370 others (ZGN), as expected based on the comparative $\Delta^{10}Be_{qtz}$ values. Although the
371 uncertainties are large, Fig. 5 could be used to make first-order quantitative estimates of
372 M_{post}/M_{pre}, given some constraints on $^{10}Be_{qtz,landslide}$.
373
374 It is not possible to directly measure the $^{10}Be_{qtz,landslide}$ for the very large number (tens of
375 thousands) of Wenchuan landslides. Instead, we approach this problem by modeling the
376 $^{10}Be_{qtz}$ in each landslide using area-volume scaling relations and the theoretical decrease in
377 $^{10}Be_{qtz}$ with depth below the Earth's surface (details described in Appendix A1). Estimated
378 volume-averaged $^{10}Be_{qtz,landslide}$ for all landslide material in each catchment (Table 3) ranges
379 from 1.24±0.12 (for catchment MJY) to 1.74±0.16 x 10^4 at/g (for catchment ZGN). These
380 model-derived $^{10}Be_{qtz,landslide}$ values provide a first-order constraint for estimating M_{post}/M_{pre}
381 for each catchment (Fig. 5). M_{post}/M_{pre} values inferred on this basis range from <2 to >8,
382 depending on the catchment (Table 3). This ratio reflects an enhancement factor describing
383 the increase in sediment mass in the river system as a result of landslide inputs, based on
384 comparison before and after the earthquake. This ^{10}Be-derived M_{post}/M_{pre} enhancement
385 factor can be compared to the enhancement factor $Q_{ss\text{-}post}/Q_{ss\text{-}pre}$, calculated from the
386 change in suspended sediment flux measured at gauging stations in the Min Jiang system
387 before and after the Wenchuan earthquake (Wang et al., *in review*). For catchments where
388 both datasets are available, the variability in M_{post}/M_{pre} values from one catchment to
389 another closely mirrors the variability in $Q_{ss\text{-}post}/Q_{ss\text{-}pre,}$ and although both ratios are
390 associated with large uncertainties, the magnitude of the values for each catchment lie in
391 similar ranges. M_{post}/M_{pre} describes the change in the mass of sediment in the river channel,
392 while $Q_{ss\text{-}post}/Q_{ss\text{-}pre}$ is the change in the mass flux of sediment per unit time that is
393 transported by the river. It is perhaps not surprising that the two ratios would have similar

values, since the ^{10}Be samples were collected from sediment deposits within the active river channel. An important difference is that M_{post}/M_{pre} has been determined from $^{10}Be_{qtz}$ in the 0.25-1 mm size fraction, while $Q_{ss\text{-}post}/Q_{ss\text{-}pre}$ reflects predominantly material that is <0.25 mm (Wang et al., *in review*). The overall similarity in the values of these ratios may suggest that there is not a strong grain size bias in terms of the entrainment and transport of material from Wenchuan landslides, at least within the range of sizes of the relatively fine-grained material considered here.

The Wenchuan case illustrates that $^{10}Be_{qtz}$ mixing may help to trace the transport of sediment from landslides, where these are sufficient in scale to measurably dilute the river sediment. This approach might be able to provide information where suspended sediment concentration data are lacking (e.g. in the small catchments SCLX and SCMJ in this study, see Table 3) and can offer insights into the transport of material across a range of size fractions that may be difficult to measure directly. Propagated uncertainties from the $^{10}Be_{qtz}$ mixing are large, but uncertainties from sediment flux estimates are also large (e.g. Dadson et al., 2004; Wang et al., *in review*). A main limitation of the $^{10}Be_{qtz}$ mixing approach is that calculation of M_{post}/M_{pre} relies on the availability of $^{10}Be_{qtz}$ data (or samples) collected before major landslide events, as well as after. For our study, the lack of data for the 1-4 mm size fraction from prior to the earthquake prevents calculation of M_{post}/M_{pre} for this specific size range, although for the post-earthquake samples measured in this study, concentrations in the 1-4 mm size fraction are within 15-20% of those in the 0.25-1.0 mm size fraction. Replicating this experiment with larger grain sizes (including gravel and cobbles) could be an interesting next step.

5.4. Monitoring sediment removal by future $^{10}Be_{qtz}$ measurement

The persistence of the sediment pulse from an event like the Wenchuan earthquake depends on the timescale of sediment transport through the system, in addition to the ^{10}Be concentrations associated with "background" (i.e., non-landslide) erosion and the associated background sediment production rates (e.g. Niemi et al., 2005). By monitoring changes in $^{10}Be_{qtz}$ following a major event, it may in principle be possible to determine the processes that govern the transport and eventual evacuation of the landslide sediment wave (e.g. Benda and Dunne, 1997). The rate of removal of landslide debris can be simplified by two idealized scenarios, in which removal is either limited by supply or by transport. These scenarios provide a useful conceptual framework for considering how the ^{10}Be signal observed in this study in the Min Jiang might evolve with time in the future, at least to first-order.

We define s*upply-limited removal* as occurring when the rate of removal of sediment material is determined by the volume that is available, in other words, when total change in volume V_{ls} is limited by the supply of landslide sediment to the fluvial network. This definition means that the volume of landslide material remaining within the Longmen Shan, V_{ls}, at time *t* will depend on the volume of material available:

$$dV_{ls}/dt = -kV_{ls} = -F_{ls} \quad (2)$$

where k is a constant and F_{ls} is the removal flux (i.e. the amount of sediment transported over time interval dt). Equation 2 integrates to give:

$$\Delta V_{ls} = V_{ls0} (1-\exp(-kt)) \quad (3)$$

where V_{ls0} is the initial landslide volume following the earthquake (Fig. 6a). Sediment transport, on the other hand, should vary as the inverse of the total landslide volume (Fig. 6b).

In contrast, we define *transport-limited removal* as occurring when the rate of removal of sediment is determined by the transport capacity of the fluvial network, which is determined by factors such as grain size and hydrological flow regime. In the theoretical end-member case, this removal rate would not depend on the amount of material available to transport, so would be independent of the volume of landslide debris remaining in the catchment. The change in volume with time thus becomes:

$$dV_{ls}/dt = -F_{ls0} \quad (4)$$

where F_{ls0} is the removal flux immediately following the earthquake, yielding:

$$V_{ls} = V_{ls0} - F_{ls0}\, t \quad (5)$$

as shown in Fig. 6a. These end-member definitions of supply- versus transport-limited sediment removal provide the basis for a simple, first-order model for the evolution of landslide sediment volumes and fluxes, and associated fluvial $^{10}Be_{qtz}$.

Assuming a time window long enough to average flow conditions, and assuming that there are no long-term changes in flow conditions, the transport of material should take place within the space defined by the limits of the two end-member scenarios (see grey area in Fig. 6a). The actual time-evolution of landslide volumes and associated sediment flux would theoretically be defined by some combination of the two. For example, the system may initially be transport-limited, because of the very large initial input of landslide debris into the river system, but once the initial supply of material in the rivers has been evacuated, the removal of the landslide material may become supply-limited. This shift might result from a grain size effect, as less material becomes available in a grain size range that can be mobilized under a given flow regime (e.g. Topping et al., 2000). It could also result from a topographic effect, because many landslide deposits are adjacent to river channels, so that the toe of the deposit enters the river system quickly while other parts of the deposit are less accessible for transport (e.g. the deposit in Fig. 2). Figs. 5b and 5c illustrate an example of

a possible trajectory in which sediment removal is initially transport-limited and then becomes supply-limited, but any number of possible combinations like this may be possible. Defining such trajectories assumes that additional supply from post-seismic landslides in years following the earthquake is small relative to the coseismic input. With post-seismic landslide maps, such additional sources could be taken into account explicitly (e.g., Hovius et al., 2011).

The key point here is that the different scenarios for sediment transport have distinct implications for how they are expected to influence changes in river sediment $^{10}Be_{qtz}$ with time (see Fig. 6c). Measurement of $^{10}Be_{qtz}$ over time in the future may be able to shed light into what regulates the long-term removal of landslide debris following a major event such as the Wenchuan earthquake, while also providing quantitative insight into the longevity of the sediment pulse in the catchment system. For example, it would be valuable to know whether $^{10}Be_{qtz}$ concentrations remain low for an extended period of time (and if so, for how long) and then increase abruptly (supply-limited case), or if concentrations change more gradually over time (transport-limited case). Actual changes in $^{10}Be_{qtz}$ in the future may be highly noisy, influenced by variable background erosion and sediment supply, and by stochastic processes such as source area changes (cf. Lupker et al., 2012), so it may not be possible to distinguish between transport scenarios. Still, first-order differences might be identifiable, and information on the pattern of these changes would be valuable for modeling post-earthquake sediment transport, with important implications for the persistence of sediment-related hazards.

6. Conclusions

Measurements of landslide deposits and river sediment from the Min Jiang river system provide direct empirical evidence that a major landslide-triggering event delivers low-$^{10}Be_{qtz}$

498 material to river systems, changing concentrations of ^{10}Be in quartz in fluvial sediment. Such
499 effects should be carefully considered when using cosmogenic nuclides to estimate
500 denudation rates, even in large catchments (with areas of up to 10^5 km^2), and when
501 assessing spatial variability in these rates in settings where landslides are important erosional
502 agents. Although the dilution of $^{10}Be_{qtz}$ introduces complications for deriving information
503 about denudation rates, it also has the potential to provide a new tool to trace the transport
504 of landslide-derived sediment. Mixing calculations provide the opportunity to estimate the
505 relative contribution of landslide material of differing grain sizes to the river sediment. The
506 challenges in determining the representative ^{10}Be concentrations in landslide material,
507 together with the effect of propagated uncertainties, may be the primary limitation in the
508 application of this approach, and more data from further studies will clearly be needed to
509 test it rigorously. In the case of the Min Jiang and its tributaries, mixing calculations suggest
510 that enhancement of sediment flux after the earthquake has been similar in the 0.25-1 mm
511 bedload size fraction and in the suspended sediment (predominantly <0.25 mm) fraction. In
512 addition to providing information about active transport processes, the capacity of $^{10}Be_{qtz}$ to
513 trace landslide sediment inputs may open the possibility of looking for variability in $^{10}Be_{qtz}$ in
514 sedimentary archives as a record of past variability in landslides and their triggers (e.g.,
515 earthquakes). Further work would be needed to confirm whether variability in $^{10}Be_{qtz}$
516 obfuscates the signal associated with landslide sediment transport. Future applications are
517 best suited to other systems where the scale of change in river sediment $^{10}Be_{qtz}$ is likely to be
518 as significant as in the Min Jiang, and this depends on factors such as event return time and
519 magnitude, landslide spatial distribution, and catchment size (e.g. Niemi et al., 2005;
520 Yanites et al., 2009).
521
522
523

Acknowledgements

This work was funded by NSF EAR-GLD Grant 1053504 to AJW, who received additional support from CAS YIS Fellowship 2011Y2ZA04. The research benefited from discussions with Niels Hovius, Vincent Godard, and Kate Huntington. Yi Long and Wei Fangqiang of the IMHE CAS, Chengdu, and Jin Wang at the IEE CAS, Xi'an, provided invaluable assistance for the fieldwork. We thank Anne Niehus for sample preparation and Peter Kubik (ETH Zurich) for the AMS measurements. The manuscript benefited significantly from constructive comments from two anonymous reviewers.

Appendix A1: Calculating an estimated average ^{10}Be composition of landslide material in each catchment

Section 5.3 of the main text considers the question of using ^{10}Be as a tracer of the amount of sediment material that has been input to the river system from coseismic landslides. This requires an estimate of the mass-weighted $^{10}Be_{qtz,landslide}$ for each catchment area considered. In this appendix, we develop a model framework for calculating the $^{10}Be_{qtz}$ in each landslide using area-volume scaling relations and the theoretical decrease in $^{10}Be_{qtz}$ with depth below the Earth's surface. We then use the $^{10}Be_{qtz,landslide}$ for each landslide to determine relevant values for each catchment.

The area A of each landslide is known from mapping using remote-sensing imagery, and corresponding volume V is calculated based on power-law area-volume scaling ($V = \alpha A^{\gamma}$), where α, γ are parameters defined by global datasets ($\log_{10}(\alpha) = -1.131$, $\gamma = 1.45 \pm 0.01$ from Guzzetti et al., 2009). Mean depth d for each landslide is determined as $d = V/A$.

For the mapped location of each landslide (elevation, latitude, longitude), we calculate a theoretical steady-state $^{10}Be_{qtz}$ vs depth curve. Assuming steady state denudation, the ^{10}Be concentration C at depth z (cf. Fig. 2b of the main text) can be represented as (Lal, 1991):

$$C(z) = \sum_i \frac{P_i(0)}{\lambda + \rho\varepsilon/\Lambda_i} e^{-z\rho/\Lambda_i} \quad \text{(A1)}$$

where i denotes each production pathway (neutrons and muons), $P_i(0)$ is the production via pathway i at the surface (i.e., z=0), λ is the ^{10}Be decay constant, ρ is the density of eroding rock, ε is the steady-state denudation rate, and Λ_i is the attenuation length associated with production pathway i. We use ρ=2.3 g/cm^3 and erosion rate ε defined by the measured pre-earthquake denudation rate in each catchment (from Ouimet et al., 2009; Godard et al., 2010). Here, we use two terms in Equation A1. For neutrons, we use Λ_n=160 g/cm^2 (a widely adopted value; cf. Goethals et al., 2009) and P_0 calculated for the latitude, longitude,

and elevation of each landslide site based on scaling of a sea level high latitude production rate by neutrons of 4.49 at g^{-1} yr^{-1} (Stone 2000; using code of Balco et al., 2008). For muons, we use $\Lambda_m = 4200$ g/cm^2 (the median value from the compilation of Braucher et al., 2013) and P_0 calculated for the elevation of each landslide site based on scaling of a sea level high latitude production rate by neutrons of 0.028 at g^{-1} yr^{-1} (Braucher et al., 2011, 2013). We also calculated the results from Equation A1 with muonic production defined by the best fit to the depth-production trends of Heisinger et al. (2002a,b) using five exponential terms (e.g., Hidy et al., 2010); this muon production calculation leads to slightly different profiles of ^{10}Be concentration vs. depth but does not change our overall conclusions.

We sum the ^{10}Be inventory over the depth above d (the landslide depth) and across area A (landslide area) to give a total $^{10}Be_{qtz}$ for each landslide. There are a number of assumptions in using Equation A1 to infer landslide $^{10}Be_{qtz}$. One is that the profile calculated using Equation A1 is for steady-state denudation; this may be valid if erosion rates have been constant at each landslide site over long enough time scale (approximately 2000-3000 years) to reach steady state, but would be violated if prior hillslope failure had cleared surface material within that time frame. Even if the depth profiles at each landslide site had reached steady state prior to the Wenchuan earthquake, we assume a spatial uniform denudation rate within each catchment, which is not likely to represent all landslide sites. However, spatial variability is expected to average over the very large number of landslides (100s to 1000s) in each catchment. Our simple approach also ignores effects such as density differences, variability in the area-volume scaling relationship, topographic shielding of cosmic rays, and landslide geometry, all of which may vary from site to site. Nonetheless, our simple model provides a first-order estimate of the $^{10}Be_{qtz}$ that might reasonably be expected for widely distributed landslides across the catchment areas. More data would clearly be needed to rigorously validate this approach, but for the one landslide with

measured concentrations, the predicted volume-averaged $^{10}Be_{qtz}$ from our simple model is $1.17+0.16/-0.13 \times 10^4$ at/g. Since the model result is based on theory, it is encouraging that the predicted average $^{10}Be_{qtz}$ lies in the middle of the range of measured values for material from the landslide deposit, and that the predicted depth curve is consistent with the observed data (cf. Fig. 2 of main text).

To determine the volume-averaged $^{10}Be_{qtz,landslide}$ for all landslide material in each catchment, we summed the ^{10}Be inventory calculated for each landslide using Equation A1 and divided by the total volume of all the landslides in the catchment. For the large catchment sites (MJY, YZX, and ZGN), we restrict the analysis to landslides <50 km along flow directions from the sampling sites. This window captures the vast majority of landslides (Figs. 4b,c of main text) but excludes the landslides that are far from the sampling site and at very different latitudes and elevations, and are thus characterized by very different ^{10}Be production rates. A more complete sediment routing model would explicitly account for sediment transport distances and would be a valuable further research effort.

599 **References**

600 Anderson, R.S., Repka, J.L., Dick, G.S., 1996. Explicit treatment of inheritance in dating
601 depositional surfaces using in situ ^{10}Be and ^{26}Al. Geology 24, 47 –51.

602 Attal, M., Lavé, J., 2006. Changes of bedload characteristics along the Marsyandi River
603 (central Nepal): Implications for understanding hillslope sediment supply, sediment load
604 evolution along fluvial networks, and denudation in active orogenic belts. Geological
605 Society of America Special Papers 398, 143–171.

606 Balco, G., Stone, J.O., Lifton, N.A., Dunai, T.J., 2008. A complete and easily accessible
607 means of calculating surface exposure ages or erosion rates from ^{10}Be and ^{26}Al
608 measurements. Quaternary Geochronology 3, 174–195.

609 Benda, L., Dunne, T., 1997. Stochastic forcing of sediment supply to channel networks from
610 landsliding and debris flow. Water Resources Research 33, 2849–2863.

611 Brown, E., Stallard, R., Larsen, M., Raisbeck, G., Yiou, F., 1995. Denudation rates
612 determined from the accumulation of in situ-produced ^{10}Be in the Luquillo experimental
613 forest, Puerto Rico. Earth and Planetary Science Letters 129, 193–202.

614 Braucher, R., Bourlès, D., Merchel, S., Vidal Romani, J., Fernadez-Mosquera, D., Marti, K.,
615 Léanni, L., Chauvet, F., Arnold, M., Aumaître, G., Keddadouche, K., 2013.
616 Determination of muon attenuation lengths in depth profiles from in situ produced
617 cosmogenic nuclides. Nuclear Instruments and Methods in Physics Research Section B:
618 Beam Interactions with Materials and Atoms 294, 484–490.

619 Braucher, R., Merchel, S., Borgomano, J., Bourlès, D.L., 2011. Production of cosmogenic
620 radionuclides at great depth: A multi element approach. Earth and Planetary Science
621 Letters 309, 1–9.

622 Burchfiel, B., Chen, Z., Liu, Y., Royden, L., 1995. Tectonics of the Longmen Shan and
623 adjacent regions, central China. International Geology Review 37, 661–735.

624 Burchfiel, B., Chen, Z., 2013. Tectonics of the Southeastern Tibetan Plateau and Its
625 Adjacent Foreland. Geological Society of America Memoirs 210.

626 Chappell, J., Zheng, H., Fifield, K., 2006. Yangtse River sediments and erosion rates from
627 source to sink traced with cosmogenic ^{10}Be: Sediments from major rivers.
628 Palaeogeography, Palaeoclimatology, Palaeoecology 241, 79–94.

629 Chmeleff, J., von Blanckenburg, F., Kossert, K., Jakob, D., 2010. Determination of the ^{10}Be
630 half-life by multicollector ICP-MS and liquid scintillation counting. Nuclear Instruments

631 and Methods in Physics Research Section B: Beam Interactions with Materials and
632 Atoms 268, 192–199.

633 Cui, Y., Parker, G., Lisle, T.E., Gott, J., Hansler-Ball, M.E., Pizzuto, J.E., Allmendinger,
634 N.E., Reed, J.M., 2003a. Sediment pulses in mountain rivers: 1. Experiments. Water
635 Resources Research 39, 1239, doi:10.1029/2002WR001803.

636 Cui, Y., Parker, G., Pizzuto, J., Lisle, T.E., 2003b. Sediment pulses in mountain rivers: 2.
637 Comparison between experiments and numerical predictions. Water Resources Research
638 39, 1240, doi:10.1029/2002WR001805.

639 Dadson, S., Hovius, N., Chen, H., Dade, B., Lin, J.-C., Hsu, M.-L., Lin, C.-W., Horng, M.-J.,
640 Chen, T.-C., Milliman, J., Stark, C., 2004. Earthquake-triggered increase in sediment
641 delivery from an active mountain belt. Geology 32, 733–736.

642 Densmore, A.L., Ellis, M.A., Anderson, R.S., 1998. Landsliding and the evolution of normal-
643 fault-bounded mountains. Journal of Geophysical Research 103, 15203–15219.

644 Densmore, A.L., Ellis, M.A., Li, Y., Zhou, R., Hancock, G.S., Richardson, N., 2007. Active
645 tectonics of the Beichuan and Pengguan faults at the eastern margin of the Tibetan
646 Plateau. Tectonics 26, TC4005.

647 Densmore, A.L., Hetzel, R., Ivy-Ochs, S., Krugh, W.C., Dawers, N., Kubik, P., 2009. Spatial
648 variations in catchment-averaged denudation rates from normal fault footwalls. Geology
649 37, 1139–1142.

650 Dunai, T., 2010. Cosmogenic Nuclides: Principles, Concepts and Applications in the Earth
651 Surface Sciences. Cambridge University Press, Cambridge.

652 Godard, V., Lavé, J., Carcaillet, J., Cattin, R., Bourlès, D., Zhu, J., 2010. Spatial
653 distribution of denudation in Eastern Tibet and regressive erosion of plateau margins.
654 Tectonophysics 491, 253–274.

655 Godard, V., Burbank, D.W., Bourlès, D.L., Bookhagen, B., Braucher, R., Fisher, G.B., 2012.
656 Impact of glacial erosion on ^{10}Be concentrations in fluvial sediments of the Marsyandi
657 catchment, central Nepal. Journal of Geophysical Research 117, F03013.

658 Godard, V., Bourlès, D.L., Spinabella, F., Burbank, D.W., Bookhagen, B., Fisher, G.B.,
659 Moulin, A., Léanni, L., 2014. Dominance of tectonics over climate in Himalayan
660 denudation. Geology, in press.

661 Goethals, M.M., Hetzel, R., Niedermann, S., Wittmann, H., Fenton, C.R., Kubik, P.W.,
662 Christl, M., von Blanckenburg, F., 2009. An improved experimental determination of

cosmogenic $^{10}Be/^{21}Ne$ and $^{26}Al/^{21}Ne$ production ratios in quartz. Earth and Planetary Science Letters 284, 187–198.

Gorum, T., Fan, X., van Westen, C.J., Huang, R.Q., Xu, Q., Tang, C., Wang, G., 2011. Distribution pattern of earthquake-induced landslides triggered by the 12 May 2008 Wenchuan earthquake. Geomorphology 133, 152–167.

Granger, D., Kirchner, J., Finkel, R., 1996. Spatially Averaged Long-Term Erosion Rates Measured from in Situ-Produced Cosmogenic Nuclides in Alluvial Sediment. The Journal of Geology 104, 249–257.

Guzzetti, F., Ardizzone, F., Cardinali, M., Rossi, M., Valigi, D., 2009. Landslide volumes and landslide mobilization rates in Umbria, central Italy. Earth and Planetary Science Letters 279, 222–229.

Hao, K., Si, H., Fujiwara, H., Ozawa, T., 2009. Coseismic surface-ruptures and crustal deformations of the 2008 Wenchuan earthquake Mw7.9, China. Geophysical Research Letters 36, L11303, doi: 10.1029/2009GL037971.

Heimsath, A.M., Dietrich, W.E., Nishiizumi, K., Finkel, R.C., 1997. The soil production function and landscape equilibrium. Nature 388, 358–361.

Heisinger, B., Lal, D., Jull, A.J.., Kubik, P., Ivy-Ochs, S., Neumaier, S., Knie, K., Lazarev, V., Nolte, E., 2002. Production of selected cosmogenic radionuclides by muons: 1. Fast muons. Earth and Planetary Science Letters 200, 345–355.

Heisinger, B., Lal, D., Jull, A.J.T., Kubik, P., Ivy-Ochs, S., Knie, K., Nolte, E., 2002. Production of selected cosmogenic radionuclides by muons: 2. Capture of negative muons. Earth and Planetary Science Letters 200, 357–369.

Hidy, A.J., Gosse, J.C., Pederson, J.L., Mattern, J.P., Finkel, R.C., 2010. A geologically constrained Monte Carlo approach to modeling exposure ages from profiles of cosmogenic nuclides: An example from Lees Ferry, Arizona. Geochemistry Geophysics Geosystems 11, Q0AA10. doi:10.1029/2010GC003084.

Hilton, R.G., Galy, A., Hovius, N., Kao, S.-J., Horng, M.-J., Chen, H., 2012. Climatic and geomorphic controls on the erosion of terrestrial biomass from subtropical mountain forest. Global Biogeochemical Cycles 26, GB3014. doi:10.1029/2012GB004314.

Hovius, N., Stark, C., Allen, P., 1997. Sediment flux from a mountain belt derived by landslide mapping. Geology 25, 231–234.

694 Hovius, N., Meunier, P., Lin, C.-W., Chen, H., Chen, Y.-G., Dadson, S., Horng, M.-J., Lines,
695 M., 2011. Prolonged seismically induced erosion and the mass balance of a large
696 earthquake. Earth and Planetary Science Letters 304, 347–355.

697 Huang, R., Fan, X., 2013. The landslide story. Nature Geoscience 6, 325–326.

698 Jarvis, A., Reuter, H.I., Nelson, E., Guevara, E., 2008. Hole-filled SRTM for the globe
699 Version 4, available from the CGIAR-CSI SRTM 90m Database
700 (http://srtm.csi.cgiar.org).

701 Kober, F., Hippe, K., Salcher, B., Ivy-Ochs, S., Kubik, P.W., Wacker, L., Hählen, N., 2012.
702 Debris-flow–dependent variation of cosmogenically derived catchment-wide denudation
703 rates. Geology 40, 935–938.

704 Kohl, C.., Nishiizumi, K., 1992. Chemical isolation of quartz for measurement of in-situ -
705 produced cosmogenic nuclides. Geochimica et Cosmochimica Acta 56, 3583–3587.

706 Korschinek, G., Bergmaier, A., Faestermann, T., Gerstmann, U.C., Knie, K., Rugel, G.,
707 Wallner, A., Dillmann, I., Dollinger, G., von Gostomski, C.L., Kossert, K., Maiti, M.,
708 Poutivtsev, M., Remmert, A., 2010. A new value for the half-life of ^{10}Be by Heavy-Ion
709 Elastic Recoil Detection and liquid scintillation counting. Nuclear Instruments and
710 Methods in Physics Research Section B: Beam Interactions with Materials and Atoms
711 268, 187–191.

712 Kubik, P.W., Christl, M., 2010. ^{10}Be and ^{26}Al measurements at the Zurich 6 MV Tandem
713 AMS facility. Nuclear Instruments and Methods in Physics Research Section B: Beam
714 Interactions with Materials and Atoms 268, 880–883.

715 Larsen, I.J., Montgomery, D.R., Korup, O., 2010. Landslide erosion controlled by hillslope
716 material. Nature Geoscience 3, 247–251.

717 Li, G., West, A.J., Densmore, A.L., Jin, Z., Parker, R.N., Hilton, R.G., 2014. Seismic
718 mountain building: Landslides associated with the 2008 Wenchuan earthquake in the
719 context of a generalized model for earthquake volume balance. Geochemistry Geophysics
720 Geosystems in press, doi:10.1002/2013GC005067.

721 Macklin, M.G., Lewin, J., 2003. River sediments, great floods and centennial-scale Holocene
722 climate change. Journal of Quaternary Science 18, 101–105.

723 Niemi, N., Oskin, M., Burbank, D., Heimsath, A., Gabet, E., 2005. Effects of bedrock
724 landslides on cosmogenically determined erosion rates. Earth and Planetary Science
725 Letters 237, 480–498.

Nishiizumi, K., Imamura, M., Caffee, M.W., Southon, J.R., Finkel, R.C., McAninch, J., 2007. Absolute calibration of ^{10}Be AMS standards. Nuclear Instruments and Methods in Physics Research Section B: Beam Interactions with Materials and Atoms 258, 403–413.

Ouimet, W., Whipple, K., Granger, D., 2009. Beyond threshold hillslopes: Channel adjustment to base-level fall in tectonically active mountain ranges. Geology 37, 579–582.

Ouimet, W.B., 2010. Landslides associated with the May 12, 2008 Wenchuan earthquake: Implications for the erosion and tectonic evolution of the Longmen Shan. Tectonophysics 491, 244–252.

Ouimet, W., Whipple, K., Royden, L., Reiners, P., Hodges, K., Pringle, M., 2010. Regional incision of the eastern margin of the Tibetan Plateau. Lithosphere 2, 50–63.

Parker, R.N., Densmore, A.L., Rosser, N.J., de Michele, M., Li, Y., Huang, R., Whadcoat, S., Petley, D.N., 2011. Mass wasting triggered by the 2008 Wenchuan earthquake is greater than orogenic growth. Nature Geoscience 4, 449–452.

Portenga, E., Bierman, P.R., 2011. Understanding Earth's eroding surface with ^{10}Be. GSA Today 21, 4–10.

Ren, Z., Zhang, Z., Dai, F., Yin, J., Zhang, H., 2013. Co-seismic landslide topographic analysis based on multi-temporal DEM--A case study of the Wenchuan earthquake. SpringerPlus 2, 544.

Robert, A., Pubellier, M., de Sigoyer, J., Vergne, J., Lahfid, A., Cattin, R., Findling, N., Zhu, J., 2010. Structural and thermal characters of the Longmen Shan (Sichuan, China). Tectonophysics 491, 165–173.

Scherler, D., Bookhagen, B., Strecker, M.R., 2013. Tectonic control on ^{10}Be-derived erosion rates in the Garhwal Himalaya, India. Journal of Geophysical Research Earth Surface 2013JF002955.

Stone, J.O., 2000. Air pressure and cosmogenic isotope production. Journal of Geophysical Research 105, 23753–23759.

Topping, D.J., Rubin, D.M., Vierra, L.E., 2000. Colorado River sediment transport: 1. Natural sediment supply limitation and the influence of Glen Canyon Dam. Water Resources Research 36, 515–542.

Vassallo, R., Ritz, J.-F., Carretier, S., 2011. Control of geomorphic processes on ^{10}Be concentrations in individual clasts: Complexity of the exposure history in Gobi-Altay range (Mongolia). Geomorphology 135, 35–47.

758 Von Blanckenburg, F., 2006. The control mechanisms of erosion and weathering at basin
759 scale from cosmogenic nuclides in river sediment. Earth and Planetary Science Letters
760 242, 224–239.

761 Wang, J., Jin, Z.D, Hilton, R.G., Zhang, F., Densmore, A.L., Li, G., West, A.J., *in review*.
762 The chronic hazard of sediment mobilized by earthquake-triggered landslides in a
763 continental mountain belt. Geology.

764 West, A.J., Galy, A., Bickle, M., 2005. Tectonic and climatic controls on silicate weathering.
765 Earth and Planetary Science Letters 235, 211–228.

766 Wobus, C., Heimsath, A., Whipple, K., Hodges, K., 2005. Active out-of-sequence thrust
767 faulting in the central Nepalese Himalaya. Nature 434, 1008–1011.

768 Xu, C., Xu, X., Yao, X., Dai, F., 2013. Three (nearly) complete inventories of landslides
769 triggered by the May 12, 2008 Wenchuan Mw 7.9 earthquake of China and their spatial
770 distribution statistical analysis. Landslides 1–21, doi: 10.1007/s10346-013-0404-6.

771 Yanites, B.J., Tucker, G.E., Anderson, R., 2009. Numerical and analytical models of
772 cosmogenic radionuclide dynamics in landslide-dominated drainage basins. Journal of
773 Geophysical Research 114, F01007, doi: 10.1029/2008JF001088.

774 Yanites, B.J., Tucker, G.E., Hsu, H.-L., Chen, C., Chen, Y.-G., Mueller, K.J., 2011. The
775 influence of sediment cover variability on long-term river incision rates: An example from
776 the Peikang River, central Taiwan. Journal of Geophysical Research 116, F03016.

777 Yanites, B.J., Tucker, G.E., Mueller, K.J., Chen, Y.-G., 2010. How rivers react to large
778 earthquakes: Evidence from central Taiwan. Geology 38, 639–642.

779 Zhang, H., Zhang, P., Kirby, E., Yin, J., Liu, C., Yu, G., 2011. Along-strike topographic
780 variation of the Longmen Shan and its significance for landscape evolution along the
781 eastern Tibetan Plateau. Journal of Asian Earth Sciences 40, 855–864.

782

TABLE 1. ^{10}Be concentrations in quartz from stream sediment and landslide deposit in the area of the 2008 Wenchuan earthquake, China

Sample ID	Description	Date of collection	Sample elevation (m)	Catchment elevation[a] (m)	Latitude WGS 84 (31°N)	Longitude WGS 84 (103°E)	Grain size (mm)	^{10}Be concentration[b] (10^4 at/g)	error[c] (1σ)
Stream sediment samples									
JWS 09-04	Yuzixi at Yingxiu	Mar-09	974	3545	03' 47.6"	28' 59.0"	0.25-1.0	2.34	±0.24
JWS 09-05	Min Jiang below Yingxiu	Mar-09	974	3491	02' 45.3"	28' 27.8"	0.25-1.0	1.58	±0.16
JWS 10-09	Same site as WBO-05-1[d]	Apr-10	1568	2833	31' 31.5"	31' 11.0"	0.25-1.0	3.12	±0.36
JWS 10-10	Zagunao at Wenchuan	Apr-10	1351	3617	29' 23.2"	34' 49.4"	0.25-1.0	3.13	±0.33
JWS 10-11	Min Jiang above Wenchuan	Apr-10	1338	3516	28' 56.0"	36' 07.8"	0.25-1.0	3.25	±0.33
JWS 10-15	Same site as WBO-04-24[d]	Apr-10	1409	2673	16' 05.2"	30' 48.5"	0.25-1.0	3.65	±0.35
JWS 10-19	Similar site to JWS 09-04	Apr-10	997	3545	04' 12.3"	28' 00.8"	0.25-1.0	1.38	±0.21
JWS 10-20	Similar site to JWS 09-05	Apr-10	974	3491	02' 42.7"	28' 28.2"	0.25-1.0	1.91	±0.23
JWS 10-09	Same as above	Apr-10	1568	2833	31' 31.5"	31' 11.0"	1.0-4.0	2.50	±0.29
JWS 10-10	Same as above	Apr-10	1351	3615	29' 23.2"	34' 49.4"	1.0-4.0	2.53	±0.31
JWS 10-19	Same as above	Apr-10	997	3545	04' 12.3"	28' 00.8"	1.0-4.0	1.16	±0.35
Samples from landslide near Yingxiu									
JWS 09-01	Bedrock sample from scar	Mar-09	1025	--	03' 56.3"	29' 6.7"	bedrock	0.17	±0.07
JWS 09-02	Top of landslide deposit	Mar-09	1016	--	03' 56.3"	29' 6.7"	0.25-2.0	0.95	±0.12
JWS 09-03	Base of landslide deposit	Mar-09	1011	--	03' 56.3"	29' 6.7"	0.25-2.0	2.14	±0.21

[a] Mean elevation of catchment upstream from sample location

[b] The blank-corrected ^{10}Be concentrations are normalized to ETH standard S2007N, which has a nominal ^{10}Be/^{9}Be ratio of 28.1 x 10^{-12} (Kubik and Christl, 2010) considering the ^{10}Be half-life of 1.387 Ma (Chmeleff et al., 2010; Korschinek et al., 2010). The secondary standard S2007N has been calibrated to the primary standard ICN 01-5-1 (Nishiizumi et al., 2007; Kubik and Christl 2010)

[c] Propagated analytical errors (1σ) include the error based on the AMS counting statistics and the error of the blank correction, but not the systematic uncertainty of the secondary standard S2007N, which is 2.7% (Kubik and Christl, 2010)

[d] Sample sites from Ouimet et al. (2009)

783

784

TABLE 2. Pre- versus post-earthquake ^{10}Be concentrations in quartz from stream sediment

Site and sample	Date sample collected	^{10}Be conc. (10^4 at/g)	1σ error (10^4 at/g)
(A) Min Jiang at Yingxiu (MJY)			
Godard LM254[a]	Spring 2004	6.03	0.86
Godard SC086[a]	Fall 2005	5.02	1.52
JWS09-05	Spring 2009	1.58	0.16
JWS10-20	Spring 2010	1.91	0.23
	Δ^{10}Be	**-3.78**	**0.39**
(B) Yuzixi at Yingxiu (YZX)			
Godard LM253[a]	Spring 2004	4.49	0.88
Godard SC082[a]	Fall 2005	4.88	0.92
JWS09-04	Spring 2009	2.34	0.24
JWS10-19	Spring 2010	1.16	0.35
	Δ^{10}Be	**-2.94**	**0.79**
(C) Zagunao at Sangping (ZGN)			
Godard LM259[a]	Spring 2004	4.32	1.26
JWS10-10	Spring 2010	3.13	0.33
	Δ^{10}Be	**-1.19**	**1.30**
(D) Min Jiang above Wenchuan (MJW)			
Godard LM261[a]	Spring 2004	2.71	1.36
JWS10-11	Spring 2010	3.25	0.33
	Δ^{10}Be	**0.54**	**1.40**
(E) Small catchment on road to Lixian (SCLX)			
Ouimet WBO-05-1[b]	2005	8.96	0.36
JWS10-09	Spring 2010	3.11	0.36
	Δ^{10}Be	**-5.85**	**0.51**
(F) Small catchment along Min Jiang (SCMJ)			
Ouimet WBO-04-24[b]	2004	6.65	0.34
JWS10-15	Spring 2010	3.65	0.35
	Δ^{10}Be	**-3.00**	**0.49**

[a] Godard et al. (2010); [b] Ouimet et al. (2009).

785

TABLE 3. Landslide densities, Δ^{10}Be values (for 0.25-1.0 mm grain size), and M_{post}/M_{pre} by catchment

Catchment	Δ^{10}Be ± 1σ (10^4 at/g)	$^{10}Be_{qtz,\ landslide}$ [a] (10^4 at/g)	M_{post} / M_{pre} [b]	$Q_{ss\text{-}post}$ / $Q_{ss\text{-}pre}$ [c]	Catchment area (km^2)	Landslide area (km^2)	Landslide areal density (%)	Max. incremental landslide density [d] (%)
(A) Min Jiang at Yingxiu (MJY)	-3.78±0.39	1.32 ($^{+0.16}/_{-0.13}$)	9.9 ($^{+10.8}/_{-4.9}$)	>6	21773	124.7	0.57	21
(B) Yuzixi at Yingxiu (YZX)	-2.94±0.79	1.15 ($^{+0.13}/_{-0.12}$)	5.9 ($^{+4.0}/_{-2.7}$)	4 to 6	1736	55.0	3.17	38
(C) Zagunao at Sangping (ZGN)	-1.19±1.30	1.94 ($^{+0.22}/_{-0.20}$)	2.0 ($^{+0.9}/_{-0.7}$)	1 to 2	4617	13.1	0.28	1.7
(D) Min Jiang above Wenchuan (MJW)	0.54±1.40	n.d.[e]	n.d.[e]	n.a.[f]	14210	12.4	0.09	9.6
(E) Small catchment on road to Lixian (SCLX)	-5.85±0.51	3.54 ($^{+0.41}/_{-0.36}$)	>10	n.a.[f]	19.69	0.32	1.63	–
(F) Small catchment along Min Jiang (SCMJ)	-3.00±0.49	2.64 ($^{+0.30}/_{-0.27}$)	4.0 ($^{+1.8}/_{-1.0}$)	n.a.[f]	41.37	1.60	3.87	–

[a] Model calculated, volume-weighted $^{10}Be_{qtz}$ (mean ± 1σ) from landslides within the catchment area; see Appendix A1 for calculation method
[b] Based on mass balance for the 0.25-1.0 mm size fraction; calculated based on Fig. 5 for $^{10}Be_{qtz,landslide}$ estimated for each catchment
[c] Based on change in suspended sediment yield that is dominated (>95%) by material <0.25 mm (Wang et al., *in review*)
[d] The maximum landslide areal density within 3 km distance contours along direction of flow from the sampling site (see Methods section of text)
[e] Not determined
[f] No gauging station data available

Figure Captions

Figure 1. Map of the Min Jiang river basin in the Wenchuan earthquake region. Yellow polygons show landslides mapped by Li et al. (2014). Thicker river demarks the Min Jiang main stem. Stars are locations of river sediment samples for ^{10}Be analysis, colour-coded by type of sample: reds – samples from Min Jiang main stem; oranges – large tributaries of the Min Jiang; blues – low-order catchments. Colours for each site match those used in Figures 3-5. Grey diamond is the landslide sample site. Abbreviations along rivers refer to catchments in this study: MJW – Min Jiang above Wenchuan, MJY – Min Jiang main stem near Yingxiu; YZX – Yuzixi sampled above Yingxiu; ZGN – Zagunao sampled above Wenchuan.

Figure 2. (a) Photograph of the landslide deposit sampled in this study, showing position of samples for $^{10}Be_{qtz}$ analysis and measured values. $^{10}Be_{qtz}$ concentrations are highest at the base of the landslide deposit, consistent with material previously residing closest to the surface, and lowest at the bottom of the exposed scar, as expected for material that was shielded from neutrons and muons prior to hillslope failure. (b) Sketch illustrating possible failure that would generate the observed variability in $^{10}Be_{qtz}$ within the landslide scar and deposit, with predicted depth-variation based on model described in Appendix A1. More work on other landslides would be needed to determine if there are regular patterns in $^{10}Be_{qtz}$ within landslide deposits that provide information about failure dynamics.

Figure 3. Concentrations of $^{10}Be_{qtz}$ in river sediment from before (uncoloured bars) and after (coloured bars) the Wenchuan earthquake, from 6 different sites in the Min Jiang basin. Post-earthquake data were collected in this study from the 0.25-1 mm size fraction. Pre-earthquake data for the two small, first-order catchments are from Ouimet et al. (2009) who used the 0.25-0.50 mm size fraction; data for the larger rivers are from Godard et al. (2010)

who used the 0.25-1 mm size fraction. Our results show little size-dependence of $^{10}Be_{qtz}$ within these ranges. Samples for the MJY site from Godard et al. (2010) were collected upstream of the confluence with the Yuzixi while JWS samples were taken downstream, but correction for the contribution from the Yuzixi based on erosion rate and aerial extent is negligible (<2%) because of the small Yuzixi basin area. Samples from locations downstream of high landslide areal density show significant changes in $^{10}Be_{qtz}$ while samples further upstream show little change. The slight increase in $^{10}Be_{qtz}$ of the Min Jiang at Wenchuan is not statistically significant, but if this is a real difference it may be due to natural variability or anthropogenic reworking of older sediments during reconstruction efforts following the earthquake. Both small catchments (blue colours) include significant areas of landslide activity within their boundaries. Note different scale for small catchments vs. large rivers; the change in $^{10}Be_{qtz}$ after the earthquake decreases the discrepancy between large river and small catchment concentrations observed prior to the earthquake (see text).

Figure 4. (a) Landslide areal density plotted versus the change in $^{10}Be_{qtz}$ concentrations of river sediment ($\Delta^{10}Be_{qtz}$) from samples in the Min Jiang following the Wenchuan earthquake, compared to pre-earthquake values. Filled circles are for sites from the main stem and major tributaries; open circles from small first-order catchments. All sites with significant landslide activity show a decrease in measured $^{10}Be_{qtz}$, and this change is roughly correlated with the average landslide density in the catchment, although there is scatter in this correlation attributable at least in part to the location of landslides within each catchment, as shown in Figs. b and c. (b) Cumulative landslide density for each catchment, calculated for 3 km contours of distance along the flow direction upstream from the catchment outlet (see text). Highest cumulative landslide densities are close to the outlets, and the high peaks in landslide density correspond to large $\Delta^{10}Be_{qtz}$. (c) Landslide area in each catchment plotted as a function of the distance from the catchment outlet. Most landslides are close to the

catchment outlets; those catchments with greater concentrations of landslides near the outlet (slope of the curve in this plot) exhibit larger $\Delta^{10}Be_{qtz}$. In all cases catchment abbreviations are as in Tables 2 and 3.

Figure 5. Calculated ratio of the mass of river sediment after the earthquake relative to before (M_{post}/M_{pre}) as a function of the average $^{10}Be_{qtz}$ concentration of landslide inputs; see text for details. Colors are as in Figs 1, 3, & 4. Solid lines are the mean values; shaded regions show propagated 1σ uncertainty envelopes bounded by dashed lines.

Figure 6. A schematic illustration of the theoretical time evolution through a major landslide event followed by recovery, illustrating the idealized conceptual end-member cases for supply-limited and transport-limited removal of landslide debris. Actual system evolution is likely to reflect some combination of supply and transport limits, as illustrated in the grey region in (a) and by the example curve in (b) and (c). Note that many different actual curves might be possible; this is just one possibility as an illustration. (a) Evolution of landslide volume remaining in the catchment over time; (b) evolution of fluvial sediment flux; and (c) implications for ^{10}Be concentration in quartz from fluvial sediments. In the case of an event like Wenchuan, where $^{10}Be_{qtz}$ data is available from before and after the earthquake, monitoring in the future might provide an opportunity to understand what controls sediment evacuation by comparison to these theoretical trajectories.

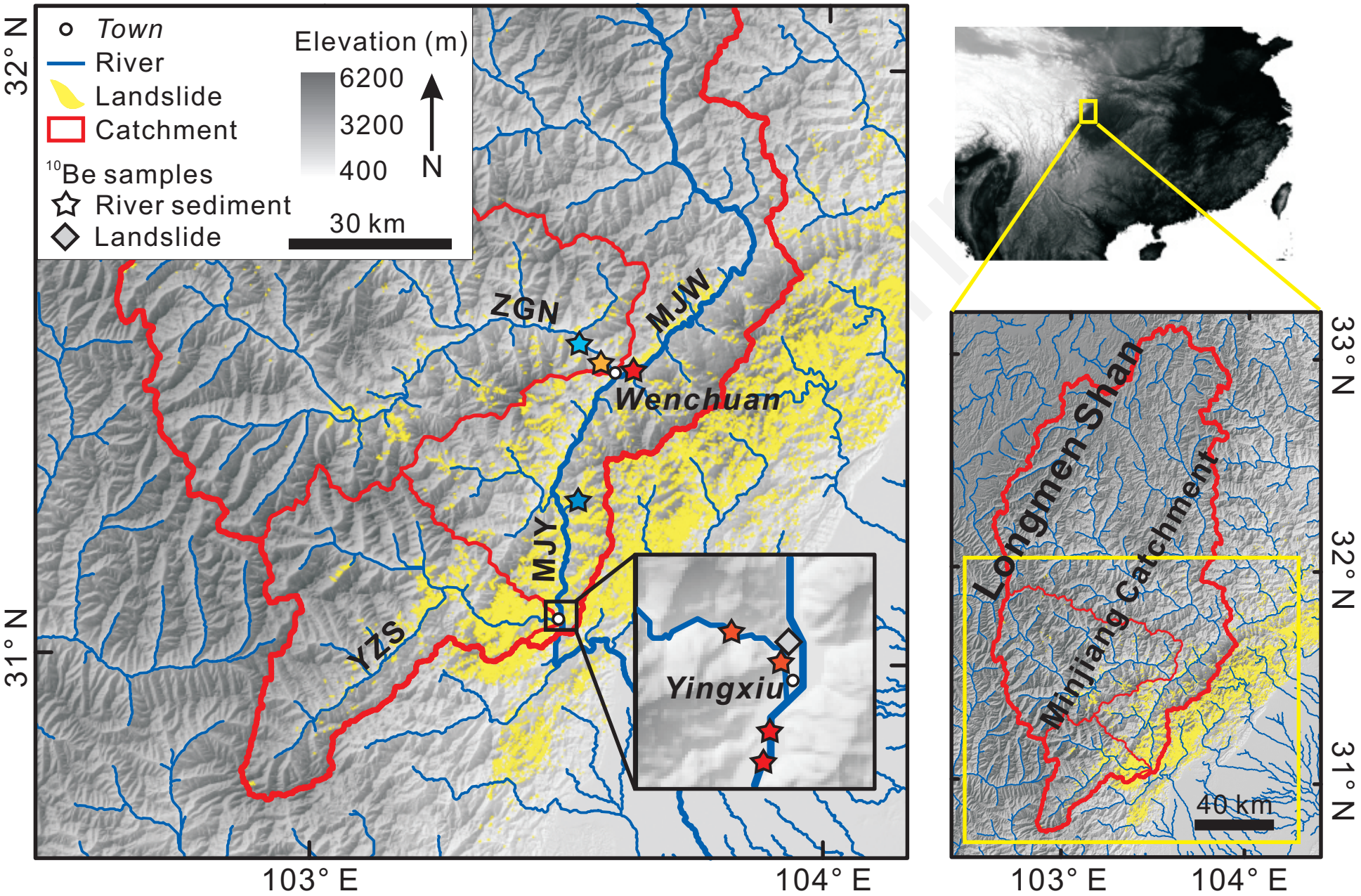
Town
River
Landslide
Catchment
10Be samples
River sediment
Landslide
Elevation (m)
6200
3200
400
N
30 km
ZGN
MJW
Wenchuan
MJY
YZS
Yingxiu
32° N
31° N
103° E
104° E
Longmen Shan
Minjiang Catchment
33° N
32° N
31° N
40 km
103° E
104° E

FIGURE 1

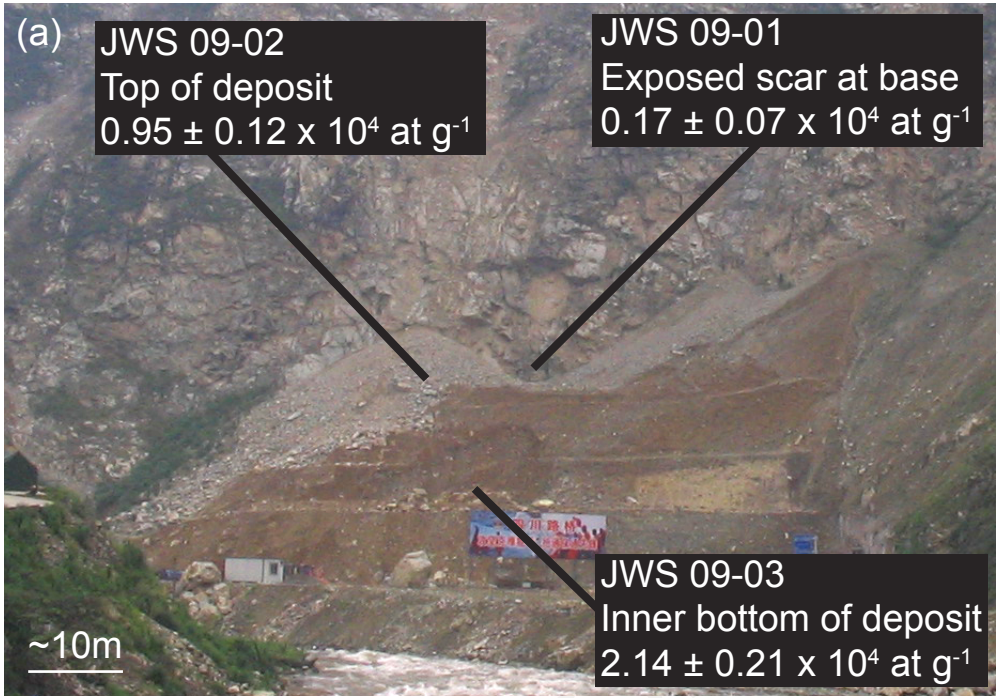
(a)
JWS 09-02
Top of deposit
0.95 ± 0.12 x 10⁴ at g⁻¹
JWS 09-01
Exposed scar at base
0.17 ± 0.07 x 10⁴ at g⁻¹
JWS 09-03
Inner bottom of deposit
2.14 ± 0.21 x 10⁴ at g⁻¹
~10m

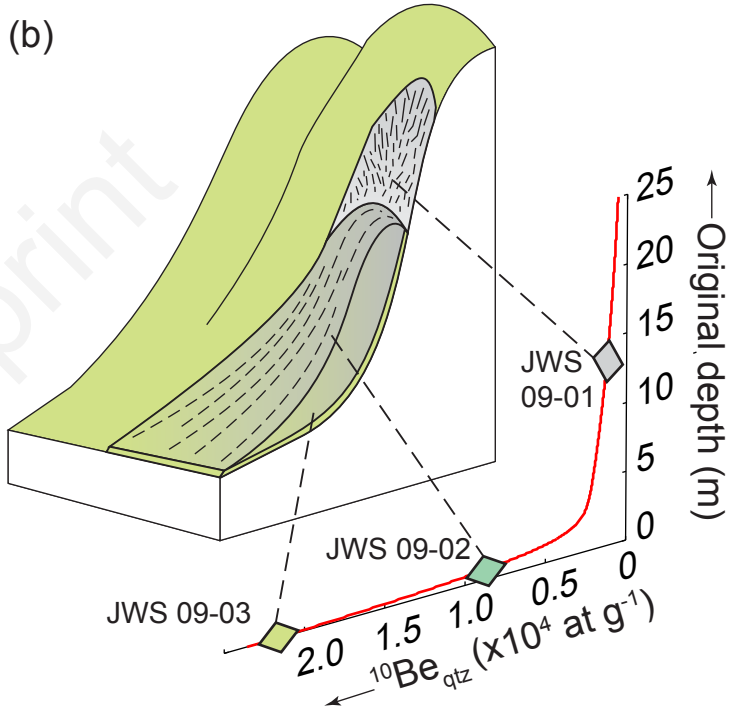
(b)
JWS 09-01
JWS 09-02
JWS 09-03
25
20
15
10
5
0
Original depth (m)
2.0
1.5
1.0
0.5
0
$^{10}Be_{qtz}$ (x10⁴ at g⁻¹)

FIGURE 2

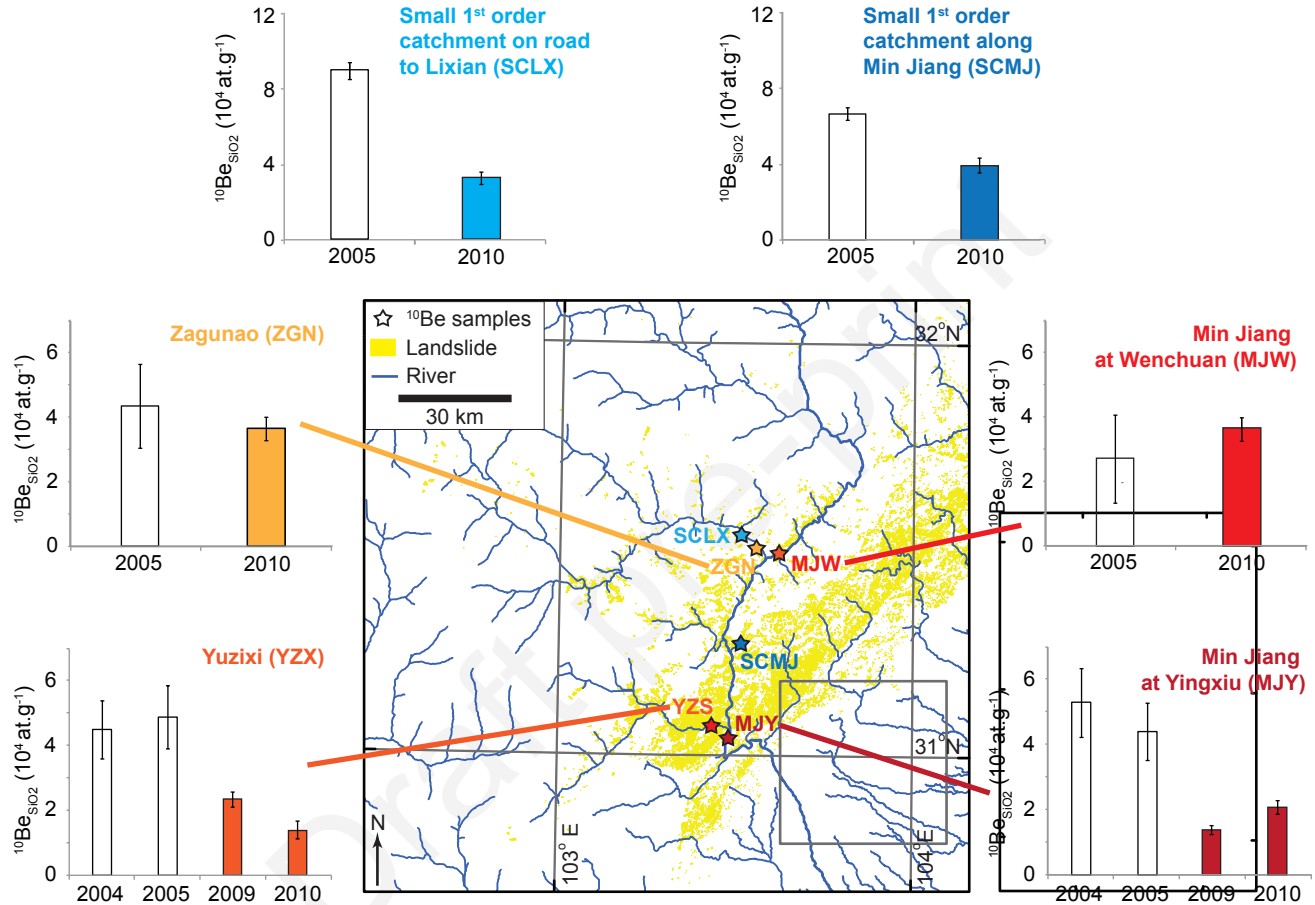
Small 1st order catchment on road to Lixian (SCLX)
Small 1st order catchment along Min Jiang (SCMJ)
Zagunao (ZGN)
Yuzixi (YZX)
Min Jiang at Wenchuan (MJW)
Min Jiang at Yingxiu (MJY)
10Be samples
Landslide
River
30 km
SCLX
ZGN
MJW
SCMJ
YZS
MJY
32°N
31°N
103° E
104° E
N
2004
2005
2009
2010

FIGURE 3

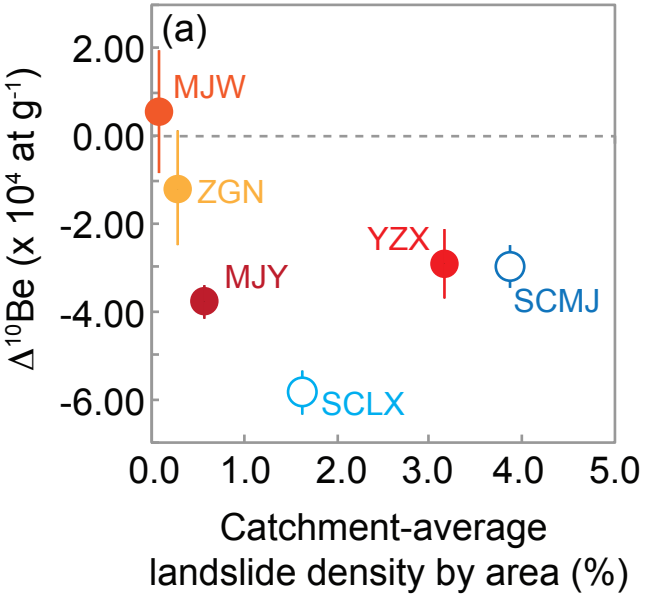

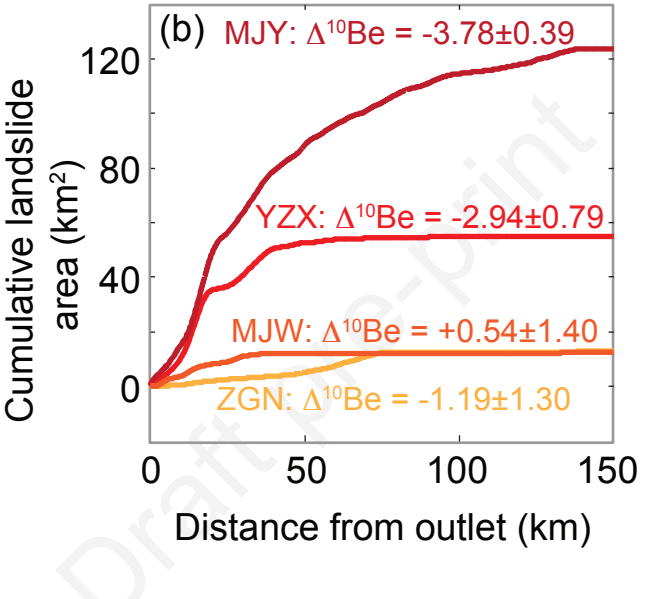

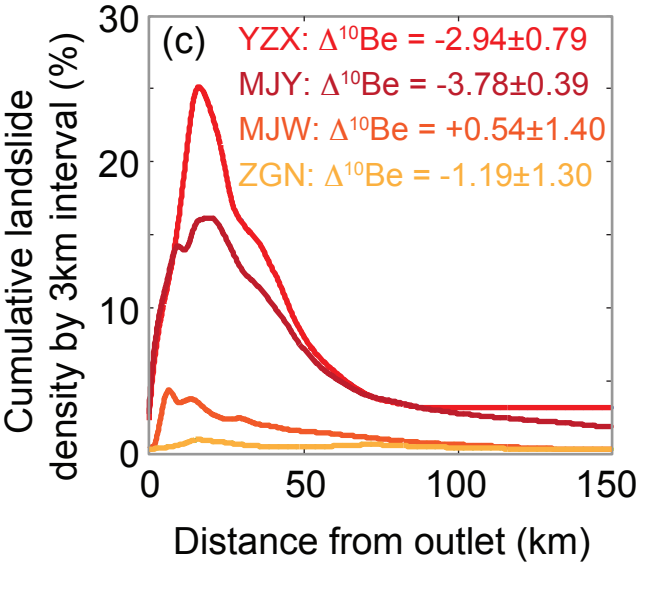

FIGURE 4

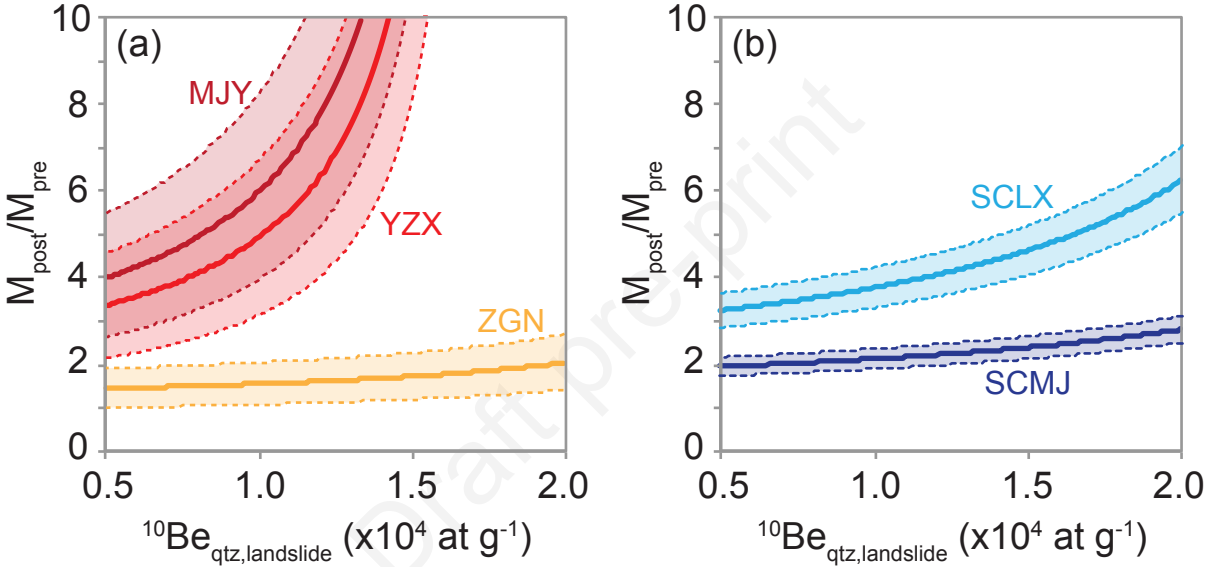

FIGURE 5

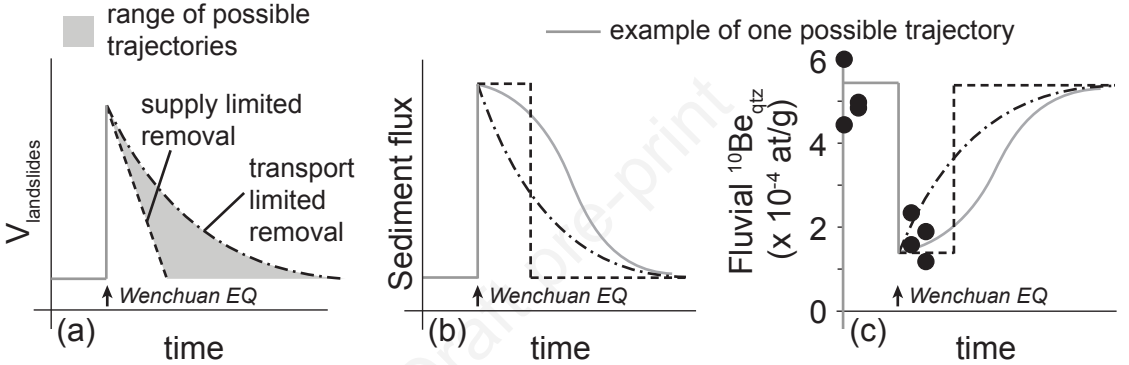

FIGURE 6